Electrotaxis-mediated cell motility and nutrient availability determine *Chlamydomonas microsphaera*-surface interactions in bioelectrochemical systems

Guowei Chen[1,5,6], Zhen Hu[1], Ali Ebrahimi[2], David R. Johnson[3], Fazhu Wu[1], Yifeng Sun[4], Renhao Shen[1], Li Liu[1], Gang Wang[4*]

[1] Department of Civil Engineering, Hefei University of Technology, Hefei 230009, China

[2] Department of Civil and Environmental Engineering, Massachusetts Institute of Technology, Cambridge, MA 02139, USA

[3] Department of Environmental Microbiology, Swiss Federal Institute of Aquatic Science and Technology, 8600 Dübendorf, Switzerland

[4] Department of Soil and Water Sciences, China Agricultural University, Beijing 100193, China

[5] Anhui Provincial Engineering Laboratory for Rural Water Environment and Resources, Hefei 230009, China

[6] Anhui Province Key Laboratory of Industrial Wastewater and Environmental Treatment, Hefei 230024, China

***Correspondences**

Gang Wang, gangwang@cau.edu.cn, **ORCID,** Gang Wang (0000-0002-3201-6950)

Graphical Abstract

Graphic abstract

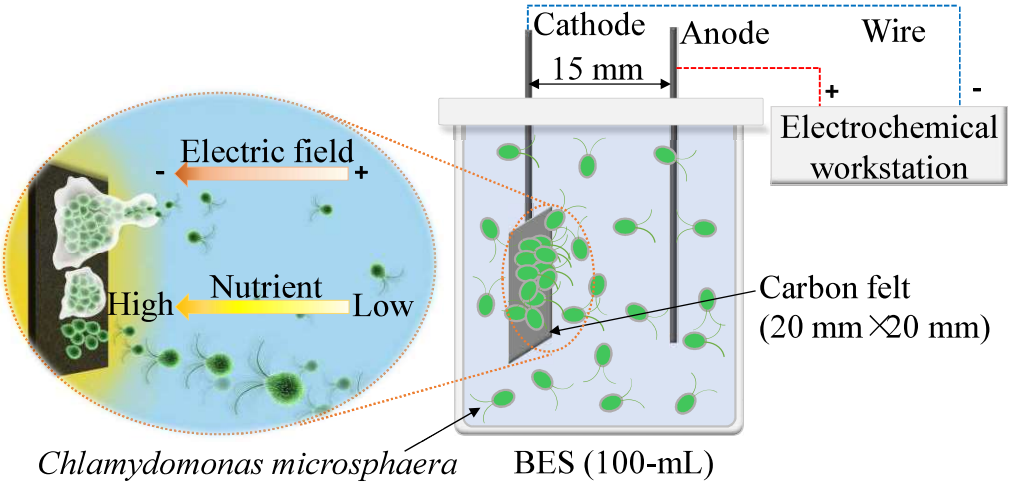

Abstract

Cell attachment onto electrode-forming biocathodes is a promising alternative to expensive catalysts used for electricity production in bioelectrochemical systems (BESs). Though BESs have been extensively studied for decades, the processes, underlying mechanisms, and determinant driving forces of microalgal biocathode formation remain largely unknown. In this study, we employed a model unicellular motile microalga, *Chlamydomonas microsphaera*, to investigate the microalgal attachment processes onto the electrode surface of a BES and to identify the determinant factors. Results showed that the initial attachment of *C. micrrosphaera* cells is determined by the applied external voltage rather than nutrient availability and occurs via electrotaxis-mediated cell motility. The subsequent development of the *C. microsphaera* biofilm is then increasingly determined by nutrient availability. Our results revealed that, in the absence of an external voltage, nutrient availability remains a dominant factor controlling the fate of the microalgal surface attachment and subsequent biofilm formation processes. Thus, our results show that electrotactic and chemotactic movements are crucial to facilitate the initial attachment and subsequent biofilm formation of *C. microsphaera* onto the electrode surfaces of BES. This study provides new insights into the mechanisms of microalgal surface attachment and biofilm formation processes on microalgal biocathodes, which hold great promise for improving the electrochemical properties of cathodes.

Keywords

Biocathode; bioelectrochemical systems; chemotaxis; electrotaxis; external voltage; microalgae

1. Introduction

Microalgae are prokaryotic or eukaryotic photosynthetic microorganisms that are often capable of rapid growth in harsh conditions due to their unicellular or simple multicellular structure [1]. Excess microalgae biomass may serve as a feedstock in an anode chamber for electricity generation in microbial fuel cells [2]. In addition, microalgae may directly participate in the anodic and cathodic reactions within photosynthetic microbial fuel cells [3,4]. Evidence suggests that the reduction of oxygen to water using an abiotic cathode as the catalyst is the limiting step for electricity production in bioelectrochemical systems (BESs), primarily because abiotic cathodes typically require expensive catalysts [5]. Microalgae biocathodes may be a promising alternative to overcome this bottleneck and reduce the costs of cathodes [6–8]. Recent studies demonstrated that enhanced and continuous current output can be achieved with microalgae biocathodes for a range of different types of microbial fuel cells (MFCs) [9], including MFCs composed of *Scenedismus obliquus, Scenedesmus quadricauda* and other mixed microalgae [6,10,11]. For example, due to the production of oxygen by a photosynthetic biofilm near a cathode surface, current output was enhanced and a maximum power density of 11 mW/m^2 was achieved for a sediment-type MFC [12].Moreover, power generation strongly depends on the rates of oxygen production at the cathode [7], where microalgae can be involved in a direct (attached cells) or indirect (with mediators) way. Obviously, microalgae attachment onto cathode will be more efficient in power production as compared to those suspended ones in cathode. For example, algae-MFC operated with *Chlamydomonas vulgaris* immobilized cathode exhibited 88% higher power density than the suspended *C. vulgaris* cathode [4], and

65 *Chlamydomonas reinhardtii* biofilm formed on the electrode was also proved to be
66 responsible for direct oxygen reduction without dosing of electron mediator [13]. It seems
67 evident that the presence of microalgae, especially attached microalgae biofilms, can
68 have a critical effect on electricity production and performance enhancement.

69 BESs are sustainable and environmentally-friendly energy technology systems that
70 employ microbes to facilitate oxidation and/or reduction reactions at the electrodes
71 (anode and cathode) [14,15], whereby the often formed electroactive biofilms on the
72 electrode surface enhance electricity generation [16]. The formation of microbial biofilms
73 on biotic and/or abiotic surfaces is ubiquitous in nature, as they facilitate nutrient
74 acquisition, enhance resistance to environmental stresses, intensify gene transfer, and
75 promote cooperation and the division of metabolic labor [17,18]. For motile
76 microorganisms, several biotic and abiotic processes influence biofilm formation on
77 surfaces, including reversible microbial attachment and detachment mediated by flagella
78 and pili followed by a transition to irreversible attachment owning to the excretion of
79 exopolysaccharides [19]. Notwithstanding the significant advancements towards a
80 fundamental understanding of microbial adhesion and the subsequent sessile life style, it
81 remains unclear how the biofilm formation process onto the electrode surfaces in BESs is
82 influenced by nutrient availability and the external applied voltage.

83 Although there have been extensive studies on the interfacial interactions and
84 underlying mechanisms of microbial adhesion to surfaces, a proper understanding of
85 microalgae attachment processes remains elusive [20]. Microalgal biofilm formation on a
86 surface is often accompanied with numerous associating microorganisms, where the
87 initial step is cell adhesion followed by subsequent biofilm development [21]. Initial

attachment is typically regulated by cell motility, Lewis acid−base interactions, and/or electro-static interactions, all of which are largely controlled by the surface characteristics of cells and abiotic substratum as well as environmental physicochemical properties such as pH and nutrients conditions [22,23]. For *C. reinhardtii,* however, surface attachment was observed to be nearly substrate independent, as cells attached to any type of surface where electrostatic interactions dominated the adhesion process [24]. In addition, eukaryotic cells often have internal sensory mechanisms enabling them to sense gradients of chemoattractant, voltage, and/or mechanical stresses, and therefore bias cell motility. As a consequence, microalgal cells may sense, respond to and move toward (or away from) an external signal, which is necessary for many biological and ecological functions [25]. Notwithstanding the numerous advances in microalgal motility characteristics, our understanding of the attachment processes of microalgal cells onto substrate surfaces and their consequent ecological functionalities remain fragmentary.

To address this knowledge gap, we studied the microalgal attachment process onto electrode surfaces under different nutrient patterns and electrical fields and identified the determinant factors. To achieve this, we performed carefully controlled laboratory experiments with single-chamber, double-electrode BES reactors consisting of pure cultures of the model unicellular motile microalga, *C. microsphaera*, which allowed us to manipulate the electrical field and nutrient availability independently and quantify the consequences. Specifically, we estimated microalgal cell numbers attached onto carbon felt, cell velocity, and nitrate and phosphate adsorption patterns onto carbon felt for different nutrient conditions and external voltages. In addition, we performed principal component analysis (PCA) to quantify the contributions of candidate driving forces,

111 including cell velocity, nitrate or phosphate adsorption, extracellular polymeric
112 substances (EPS) excretion, and zeta potential value of cells, on *C. microsphaera*
113 attachment onto carbon felt for various nitrate or phosphate concentrations and external
114 voltages.

115 **2. Materials and Methods**

116 **2.1 Strains, medium and growth condition**

117 *C. microsphaera* (FACHB 52) was obtained from the Freshwater Algae Culture
118 Collection at the Institute of Hydrobiology (Wuhan, China) and served as a model single-
119 cell green alga in this study. *C. microsphaera* inoculum cultures were obtained by
120 harvesting cells at the mid-log phase by centrifugation (5810R, Eppendorf, Hamburg,
121 Germany) at 2000×g for 10 min, washing twice with deionized water, and then
122 resuspended in deionized water to a finial cell density of ~ 1.0×10^6 cells/mL.
123 Experiments were performed in triplicate if not specifically indicated otherwise. For all
124 experiments, the inoculum cultures were diluted at 10% ($V_{inoculum}/V_{medium}$) in 500 mL
125 Erlenmeyer flasks containing 250 mL of sterile Bristol's solution and grown in a climate
126 chamber (BDP-250CO2, BaiDianTech, China) at 25 ± 1°C and 2000 lux illumination
127 intensity with a 12-12 h light-dark cycle. Cell growth was monitored by measuring the
128 optical density at 680 nm using a UV-vis spectrophotometer (Unico, Shanghai). Sterile
129 Bristol's solution was used for all cell culturing and consists of (in mg/L): $NaNO_3$, 250.0;
130 K_2HPO_4, 75.0; $MgSO_4\cdot7H_2O$, 75.0; $CaCl_2\cdot2H_2O$, 25.0; KH_2PO_4, 175.0; NaCl, 25.0;
131 $FeCl_3\cdot6H_2O$, 5.0; H_3BO_3, 2.86; $MnCl_2\cdot4H_2O$, 1.86; $ZnSO_4\cdot7H_2O$, 0.22; $Na_2MoO_4\cdot2H_2O$,
132 0.39; $CuSO_4\cdot5H_2O$, 0.08; $Co(NO_3)_2\cdot6H_2O$, 0.05. All chemicals were analytical reagent

grade and were purchased from Sinopharm Chemical Reagent Co., Ltd. (Shanghai, China).

2.2 Bioreactor assembly and configuration

Single-chamber, double-electrode BES reactors were constructed and used for experiments under voltage control conditions [26]. As depicted in **Fig. 1**, the BES reactor was a bottle-type reactor with a 100-mL working volume and sealed with a butyl rubber stopper. Two 6 mm diameter holes were milled in the stopper to allow the insertion of two plain graphite rods as electrodes (6.0 mm in diameter, 16.0 cm in height). The electrode spacing between the anode and cathode was fixed at 15 ± 2.0 mm. The graphite rod of the cathode was connected to a piece of carbon felt (20 mm × 20 mm, 4 cm^2 projected surface area) to expand its working area. The electrodes were connected to an electrochemical workstation (Corr Test CS150, Wuhan, China) by wires to supply various external voltages. Prior to experiments, the graphite rod and carbon felt were first washed three times with deionized water, then soaked in 1.0 M HCl solution followed by 1.0 M NaOH solution for 10 min to remove possible metal and biomass contaminations, and finally rinsed three times with deionized water. All reactors, electrodes, and stoppers were sterilized by autoclaving at 121°C for 15 min prior to beginning the experiments.

2.3 Nutrient adsorption at various initial concentrations and applied voltages

Nutrient adsorption onto the electrode surfaces generates hotspots for cell attachment; therefore, nutrient adsorption was assessed across a nitrite gradient (referred to as nitrite dilution series I) and a phosphate gradient (referred to as phosphate dilution series I). Nitrate dilution series I was prepared using a modified Bristol's solution where the

155 $NaNO_3$ concentration was set to 250 mg/L (standard concentration), 125 mg/L, 25 mg/L,
156 5 mg/L, 2.5 mg/L, or 0 mg/L. Similarly, phosphate dilutions series I was prepared using a
157 modified Bristol's solution where the KH_2PO_4 concentration was set to 250 mg/L
158 (standard concentration), 125 mg/L, 25 mg/L, 5 mg/L, 2.5 mg/L, or 0 mg/L. The pH
159 value of the medium was adjusted to 6.55 ± 0.01 (original pH of Bristol's solution) using
160 0.1 mol/L HCl or NaOH solution. All dilutions were autoclaved at 121°C for 15 min
161 before use. Nutrient adsorption experiments were conducted in 11 identical sterile BES
162 reactors. In each reactor, 100 mL of modified sterile Bristol's solution (dilution series I)
163 was added. Similarly, nitrate and phosphate dilution series I were also used in nutrient
164 adsorption experiments with various applied voltages. Nutrient adsorption experiments
165 were conducted in four parallel groups with external voltages of 200 mV, 400 mV, 600
166 mV and 800 mV between the two electrodes, with each group consisting of 11 sterile
167 BES reactors. In each BES reactor, 100 mL of modified sterile Bristol's solution (dilution
168 series I) was added. Samples of 1 mL were removed from each BES reactor at 0, 20 min,
169 60 min, 240 min, 480 min and 720 min for analysis. All experiments were performed at
170 2000 lux illumination intensity and 25 ± 1°C without shaking in triplicate unless
171 otherwise specified.

172 **2.4 *C. microsphaera* attachment at various initial nutrient concentrations and**
173 **applied voltages**

174 *C. microsphaera* attachment was also assessed across a nitrite gradient (referred to as
175 nitrite dilution series II) and a phosphate gradient (referred to as phosphate dilution series
176 II). Nitrate dilution series II was prepared using a modified Bristol's solution where the
177 $NaNO_3$ concentration was set to 312.5 mg/L, 156.2 mg/L, 31.2 mg/L, 6.2 mg/L, 3.1

178 mg/L, or 0 mg/L. Similarly, phosphate dilution series II was prepared using a modified
179 Bristol's solution where the KH_2PO_4 concentration was set to 312.5 mg/L, 156.2 mg/L,
180 31.2 mg/L, 6.2 mg/L, 3.1 mg/L, or 0 mg/L. The pH value of the medium was adjusted to
181 6.55 ± 0.01 using 0.1 M HCl or NaOH solution. All dilutions were autoclaved at 121°C
182 for 15 min before use. To analyze the effects of initial dilutions on microalgae
183 attachment, 30 sterile BES reactors were prepared. In each BES reactor, 40 mL of
184 modified sterile Bristol's solution (dilution series II) was added. To quantify the effects
185 of various applied voltages on microalgae attachment, four parallel groups of experiments
186 were carried out with external voltages of 200 mV, 400 mV, 600 mV or 800 mV between
187 the two electrodes. After 12h, a 10 mL microalgae inoculum at a cell density of 1.0×10^6
188 cells/mL was transferred into each BES reactor, yielding a final N or P concentration of
189 250 mg/L, 125 mg/L, 25 mg/L, 5 mg/L, 2.5 mg/L, or 0 mg/L. The pH value of the
190 medium was adjusted to 6.55 ± 0.01 using 0.1 M HCl or NaOH solution. The experiment
191 was performed in a climate chamber (BDP-250CO2, BaiDianTech, China) at 25±1°C and
192 2000 lux illumination intensity.

193 **2.5 Measurement of microalgal cell motility**

194 Thirty microliter aliquots of microalgal culture were removed from each reactor at 20
195 min, 60 min, and 720 min after incubation and were transferred to a 6-well plate for cell
196 movement tracking under identical experimental conditions. An optical inverted
197 microscope system (IX73, Olympus, Japan) equipped with a digital camera (DP73,
198 Olympus, Japan) was employed to track cell movement via video acquisition. Real-time
199 trajectories of microalgal cells were recorded at 12-15 frames/second for 60 seconds.
200 Microbial cell velocity was measured frame by frame and was calculated at a time

interval of 0.50 seconds. The average cell velocity was calculated as the mean of the complete series of trajectories [27]. For each sample, at least 100 randomly selected microalgae cells were used for motility analysis.

2.6 Staining and confocal laser scanning microscopy observations

Syto 63 (Molecular Probes, Carlsbad, CA, USA) was applied to visualize and quantify total cells [28]. Specifically, carbon felt samples were collected from each reactor at the end of the experiment and were then transferred and fixed onto a glass slide. Each sample was then mixed with 100 μL Syto 63 solution (20 μmol/L) and incubated for 30 min. The stained samples were next washed twice with phosphate-buffered saline (pH 7.2) to remove excess dye. The stained and washed samples were finally imaged using a confocal laser scanning microscope (Carl Zeiss LSM710, Germany) equipped with a 100 × oil objective. Image processing and analysis were performed using ZEN blue (version 2012, Carl Zeiss, Germany).

2.7 EPS, zeta potential and chemical analysis

EPS were extracted from microalgae cultures using a modified heat extraction method as described in a previous study [29]. Proteins (PN) were analyzed using a Folin-phenol method and a UV-vis spectrophotometer (PerkinElmer Lambda 25) at 750 nm [30]. Polysaccharides (PS) were analyzed using an anthrone colorimetric method and a UV-vis spectrophotometer (Unico, Shanghai) at 420 nm [31]. The zeta potential was measured using a zeta-potential analyzer (Nano-ZS90, Malvern, UK). Total phosphorous was measuring using an ascorbic acid method and nitrate was measured using an ultraviolet spectrophotometric screening method according to Standard Methods [32].

2.8 Statistical Analysis

All results are reported as mean values of three replicates and standard deviations of the mean (SD), except for mean cell velocity which used five replicates. Linear fitting was applied to describe the effect of applied voltage on nutrient adsorption with 95% confidence. Effects of nutrient concentrations and applied voltage on microalgal cell attachment were evaluated with one-way or two-way analysis of variance (ANOVA). Statistical significance was defined by 95% confidence intervals and was accepted at $P < 0.05$ (*), $P < 0.01$ (**) and $P < 0.001$ (***). Pearson and Spearman correlation tests were used to test pairwise correlations between factors. The general characteristics of cell attachment from various external voltages and nutrient concentrations were analyzed using PCA methods.

3. Results and discussion

3.1 *C. microsphaera* attachment under various applied voltages

External voltage loading clearly stimulated the attachment of *C. microsphaera* cells across all nitrate and phosphate concentrations (**Fig. 2**). This was further evidenced by the confocal microscopy images, indicating significantly enhanced cell attachment onto the carbon felt in original Bristol's solution (as an example) under an external voltage (**Fig. S1**). Specifically, with a 200 mV external voltage, the number of attached cells estimated at 20 min after inoculation varied between 3.46 (SD, 0.04) $\times 10^4$ cells/cm^2 and 3.97 (SD, 0.30) $\times 10^4$ cells/cm^2 across all nitrate concentration scenarios, which was 39-59% larger than those when no external voltage was applied. At 480 min elapsed time, cell attachment increased steadily, ranging from 17.04 (SD, 0.77) $\times 10^4$ cells/cm^2 to 19.37

245 (SD, 0.51) $\times 10^4$ cells/cm^2 at various initial nitrate concentrations. There was no
246 noticeable difference among the numbers of attached cells across different initial nitrate
247 concentrations, except for those for the last 720 min ($P > 0.05$ for the ANOVA test,
248 **Table S1**). However, at higher external voltage (400 mV - 800 mV), significant
249 differences were gradually observed across various initial nitrate concentration scenarios
250 as incubation progressed ($P < 0.05$ for the ANOVA test, **Table S1**). The numbers of
251 attached cells at 480 min varied among different initial nitrate concentrations from the
252 lowest values of 21.71 (SD, 2.58) $\times 10^4$ cells/cm^2, 18.63 (SD, 1.18) $\times 10^4$ cells/cm^2, and
253 13.69 (SD, 0.48) $\times 10^4$ cells/cm^2 to the highest values of 24.62 (SD, 0.88) $\times 10^4$ cells/cm^2,
254 22.32 (SD, 1.30) $\times 10^4$ cells/cm^2, and 18.32 (SD, 0.83) $\times 10^4$ cells/cm^2, for external
255 voltages of 400 mV, 600 mV and 800 mV, respectively. Similarly, the numbers of
256 attached cells varied slightly amongst various initial phosphate concentrations at the early
257 incubation time for all external voltage scenarios (**Fig. 2**). For instance, with 200 mV
258 external voltage applied, the number of attached cells at 20 min varied from 3.46 (SD,
259 0.18) $\times 10^4$ cells/cm^2 to 3.98 (SD, 0.51) $\times 10^4$ cells/cm^2 across different initial phosphate
260 concentrations. Afterwards, significant differences were found amongst different initial
261 phosphate concentrations across all external voltages, typically at incubation times of 240
262 min and longer ($P < 0.05$ for ANOVA test, **Table S1**) with the number of attached cells
263 ranging from 15.86 (SD, 0.32) $\times 10^4$ cells/cm^2 to 27.12 (SD, 0.81) $\times 10^4$ cells/cm^2 at 720
264 min after inoculation. An additional ANOVA test on the attached cell numbers showed
265 significant differences ($P < 0.01$) amongst different external voltages for all initial nitrate
266 or phosphate concentrations and different times (**Table S2**). These results indicate that

267 the external voltage likely plays a more important role on cell attachment than the initial
268 nitrate or phosphate concentrations.

269 **3.2 Nutrient adsorption under various applied voltages**

270 Besides providing a substratum for cell attachment, carbon felt might also serve as a
271 nitrate or phosphate enrichment layer that accumulates available nitrate and phosphate for
272 supporting growth of *C. microsphaera.* Under external voltage loading, the adsorption of
273 either nitrate or phosphate onto the carbon felt was globally reduced when compared to
274 the absence of an external voltage (**Fig. 3**). For all concentrations, no significant
275 differences in nitrate adsorption were found across all tested external voltages ($P > 0.05$
276 for ANOVA test). Specifically, nitrate adsorption remained within a low range of 0.01
277 mmol/L - 0.03 mmol/L and 0.01 mmol/L - 0.05 mmol/L during the entire incubation for
278 low nitrate concentrations of 5 mg/L and 2.5 mg/L, respectively. At medium nitrate
279 concentrations of 25 mg/L and 125 mg/L, nitrate adsorption was estimated in the range of
280 0.03 mmol/L to 0.16 mmol/L. As for the original 250 mg/L nitrate concentration, nitrate
281 adsorption was between 0.08 mmol/L to 0.53 mmol/L. Similarly, no significant
282 differences ($P > 0.05$ for ANOVA test) in phosphate adsorption were found among all
283 external voltage scenarios (**Fig. 3**). Similar with those for the control (0 mV), both nitrate
284 and phosphate adsorption ratios (nutrient adsorption amount to the initial nutrient supply)
285 gradually increased with incubation time, with a slightly decreased adsorption ratio at
286 higher external voltages (**Fig. S2**). In addition, Pearson and Spearman correlation
287 analyses did not detect significant correlations between cell attachment and nitrate or
288 phosphate adsorption on the carbon felts at any of the tested external voltages (**Table S3**).

289 This suggests the existence of alternative mechanisms (e.g., cell motility) other than
290 nutrient sources regulating cell attachment onto the carbon felt.

291 **3.3 External voltage loading alters cell motility patterns**

292 *C. microsphaera* cells may respond to nutrient gradients or to attractant hotspots on
293 carbon felt via chemotactic movement. Microbial motility patterns were therefore
294 quantified at various nitrate or phosphate conditions. External voltage loading clearly
295 stimulated cell velocity across all tested scenarios (**Fig. 4**). Specifically, the average cell
296 velocity in the original Bristol solution increased from 16.44 - 30.85 μm/s in the absence
297 of external voltage to 46.18 - 51.55 μm/s at an external voltage of 200 mV, with its value
298 slightly increasing up to 50.00 - 58.69 μm/s at 400 mV, and thereafter reducing down to
299 41.88 - 47.37 ± 1.51 μm/s at 800 mV. Similarly, external voltage loading under nitrate or
300 phosphate diluted conditions also yielded significantly increased cell velocities, albeit
301 with slightly reduced values as compared with the original concentrations. For instance,
302 at a nitrate concentration of 25 mg/L, the highest measured cell velocity at 400 mV was
303 52.81 μm/s, which is nearly 10% lower than that of the original nitrate concentration of
304 250 mg/L (58.69 μm/s) while still being 48% above that without voltage (35.59 μm/s).
305 When the nitrate concentration was set to 2.5 mg/L, an even more increased cell velocity
306 was measured at up to 68.55 ± 2.61 μm/s at 400 mV external voltage. Further decrease of
307 the initial nitrate concentration to zero resulted in a minor decline in cell velocity to a
308 range between 30.63 ± 1.17 μm/s and 65.77 ± 1.17 μm/s. Not surprisingly, similar
309 velocity patterns were observed for phosphate, with the highest cell velocity estimated
310 approaching 70.05 ± 1.80 μm/s at an initial phosphate concentration of 25 mg/L and an
311 external voltage of 400 mV (**Table S4**). Overall, cell velocity was promoted by the

312 presence of an external voltage regardless of the initial nitrate or phosphate
313 concentrations.

314 **3.5 Dominant factors driving *C. microsphaera* attachment with various applied**
315 **voltages under various nutrient concentrations**

316 Complex microbial cell surface characteristics (often linked to EPS excretion) are key
317 factors shaping cell-substratum interactions, and thereby promoting or interrupting cell
318 attachment patterns [33]. However, external voltage loading clearly facilitated EPS
319 production of *C. microsphaera*, with nearly equal improvement (i.e., no substantial
320 differences among various voltage loading and nitrate/phosphate concentrations) as
321 compared with those without voltage (**Fig. S3**). Pearson and spearman analysis showed
322 strong correlations between cell attachment and cell velocity for all tested concentration
323 scenarios at various applied voltages (**Table S5**).

324 Cell motility, nitrate or phosphate adsorption and EPS excretion are considered as
325 candidate factors driving cell attachment under an external voltage and nutrient limitation
326 conditions. A PCA approach, based on three representative experiments of original
327 Bristol's solution, 2.5 mg/L nitrate, and 2.5 mg/L phosphate, was employed to evaluate
328 the combined impact of these factors on shaping cell surface attachment onto the carbon
329 felt. In the original Bristol's solution, the first two extracted principal components
330 accounted for approximately 86.82% of the total variance in cell attachment amongst all
331 samples, which could explain most information on the variables. This suggests that
332 nitrate or phosphate adsorption might be the dominant factors determining cell
333 attachment in both the presence and absence of external voltages, whereas polysaccharide
334 and protein excretions were critical to cell attachment at different incubation time (**Fig.**

335 **5**). Under nitrate or phosphate limitation conditions (2.5 mg/L nitrate or phosphate), the
336 eigenvalues of axis 1 and axis 2 (i.e., PC1 and PC2) from the PCA biplot were 65.44%
337 and 22.51%, respectively, which could explain 87.95% of the multivariate variation. In
338 addition, results showed that the profiles at 0 mV and 200 mV tended to be distinct from
339 those at 400, 600 and 800 mV for both nitrate and phosphate limitation conditions (2.5
340 mg/L nitrate or phosphate). Though polysaccharide and protein excretion were still the
341 critical factors determining cell attachment at different incubation times, nitrate or
342 phosphate adsorption and cell motility likely became the main factors affecting cell
343 attachment with different external voltage loading.

344 **4. Discussion**

345 With the presence of external voltages, BES can be conducted to increase the kinetics of
346 reactions and/or to drive thermodynamically unfavorable reactions. Extensive studies
347 have been focused on the development of biocathode BES, and revealed that various
348 cathode potentials (from -0.54 V to 0.8 V) and circuit currents (from -0.45 $\mu A/mm^2$ to 2.7
349 $\mu A/mm^2$) could be achieved [34]. Our results showed that the presence of algal biofilm
350 did alter the electrode characteristics (**Fig. S4**). The application of external voltage will
351 also cause the electrophoretic movement of charged particles towards the opposite
352 polarity electrode. With the polarization of the electrodes, electrochemical reactions may
353 take place, particularly electro-oxidation of the electrodes and electrolysis of water,
354 leading to electrode corrosion and bubbling [25]. Nevertheless, the external voltage
355 applied in our study ($0 - 0.8$ V) was significantly lower than that is needed for water
356 electrolysis (2.3 V). Therefore, even without considering electrodes' overpotentials and
357 ohmic losses, there is barely electrolysis at such low voltages in our study [35]. The

358 electrolyte is another important component of BESs, which should have good
359 conductivity and excellent microbial activity [36]. Higher electrolyte conductivity
360 ascertains the better performance of BES, but the electrolyte conductivity should not go
361 beyond the tolerance level of bacteria [37]. The conductivity of wastewater can usually
362 vary from 0.2 ms/cm to 40 ms/cm. In this study, the solution conductivity varied in a
363 limited range of 0.27 ms/cm to 0.66 ms/cm, confining the impact of solution conductivity
364 on the BES performance.

365 Cell-substratum interactions are the major driving force for initial cell adhesion,
366 and the properties of the substratum, such as hydrophobicity, surface roughness, and
367 surface texture are the most important features [24,38]. In addition, microalgal cell
368 motility, nutrient availability, zeta potential, presence of bacterial populations, and other
369 environmental stresses may play critical roles in the initial adhesion of microalgal cells
370 onto substratum surfaces [21,29,39,40]. In our study, surface attachment occurred at all
371 tested nutrient levels, indicating that the surface attachment of *C. microsphaera* is a
372 substrate-independent process, which is similar with that of *C. reinhardtii* adhesion onto
373 abiotic surfaces [24]. Meanwhile, nutrient availability remarkably influenced the
374 population of attached cells, with more frequent cell attachment taking place at relatively
375 lower concentrations of nutrients. For a chemotactic microbe inhabiting a nutrient-limited
376 aqueous environment, the surface attached substances often form an ideal resource target
377 that is rich in labile nutrients. The results indicated that substratum surface-adsorbed
378 nitrate or phosphate likely acted as nutrient hotspots (as compared with that of relatively
379 lower nutrient concentration in bulk aqueous medium) for harboring *C. microsphaera*
380 cells in a nutrient-limiting environment. In addition, the limited nutrient acquisition in

bulk medium would substantially stimulate *C. microsphaera* cell velocity and promote active motility (propelled by the synchronous action of its two flagella) of *C. microsphaera* cells towards the substratum surface-adsorbed nutrient hotspots. This, in turn, would enhance cell attachment onto the substratum surface. Meanwhile, EPS may serve as carbon or energy reserves for microalgal growth and may further protect attached cells against environmental stress, thus favoring microalgae adhesion [41,42]. The results demonstrate that, in addition to the promotion of early-stage surface attachment, EPS also functions to facilitate the consequent colony development of *C. microsphaera*.

With the application of an external voltage, nutrient availability no longer becomes the dominant factor shaping surface attachment of *C. microsphaera*. Ronen et al. reported that the application of an electrical potential had a significant impact on triggering detachment of live bacterial cells, while barely influencing inactive bacterial cells or abiotic particles. Besides chemotactic movement, motile cells also exhibit increased migration speeds and directionality in gradients of electrical potential stimuli [43–45], whereby electrotaxis is the phenomenon by which cells bias their motion directionally in response to an externally applied electrical field. As we known, the zeta potential is the electrical potential at the shear plane, which is the boundary of the surrounding liquid layer attached to the moving particles in the medium. The high absolute value of the zeta potential generates a repulsive electrostatic force between particles, which is a key property of an agglomeration resistant suspension [46]. The general dividing line between stable and unstable suspensions is generally taken at either +30 or -30 mV. Particles with zeta potentials more positive than +30 mV or more negative than -30 mV are normally

404 considered stable [46,47], i.e., low absolute zeta potential values of < 30 mV likely
405 favorite cell aggregation or attachment onto substratum [48]. In this study, the absolute
406 zeta potential values of all nitrate and phosphate concentrations were smaller than 30 mV,
407 suggesting favorable conditions for cell attachment, especially under intermediate nitrate
408 or phosphate concentration (e.g., 25 mg/L) (**Fig. S5**). Therefore, zeta potential is not
409 considered as the main driving forces here. The results indicated that it was the external
410 applied voltage, rather than nutrient availability, that is crucial to the surface attachment
411 of *C. microsphaera* during the entire incubation through enhanced cell velocity. Though
412 BES has been widely studied for decades, the factors driving bioanode or biocathode
413 formation and their variability especially during startup remain unclear, leading to a lack
414 of effective strategies to initiate larger-scale systems [18]. In our study, accelerated
415 microalgal attachment occurred for medium external voltage loadings, with cell
416 electrotaxis and chemotaxis the most predominant factors driving surface attachment of
417 *C. microsphaera* cells onto the electrode surfaces. In addition, the surface attached
418 microalgal populations often have better light availability as compared with those of
419 suspended ones in bulk aqueous medium [49]. Consequently, the enhanced surface
420 attachment of microalgal populations is promising for advancing the harvest process in
421 the biofuel industry, as well as improving the electrochemical properties of cathodes.

422 **5. Conclusions**

423 In conclusion, electrotactic and chemotactic movements are crucial to facilitate the initial
424 attachment and subsequent biofilm formation of *C. microsphaera* onto the electrode
425 surfaces of BES. In the absence of an external voltage, nutrient availability is an
426 important factor controlling microalgal surface attachment and subsequent biofilm

427 formation process. However, the presence of external voltage itself, rather than nutrient
428 availability, is the predominant force leading to the initial attachment of *C.*
429 *micrrosphaera* cells via electrotaxis-mediated cell motility. The subsequent development
430 of the *C. microsphaera* biofilm is then increasingly determined by nutrient availability.
431 These quantitative estimations advance our mechanistical understanding of microalgal
432 surface attachment and biofilm formation processes on microalgal biocathodes, which
433 hold great promise for improving the electrochemical properties of cathodes and, more
434 generally, advancing the biofuel industry.

435 **Acknowledgments**

436 The authors acknowledge the financial supports of the National Natural Science
437 Foundation of China (41877412), the 2115 Talent Development Program of China
438 Agricultural University, the Chinese Universities Scientific Fund, and the Project to Attract
439 High Level Foreign Experts (G20190001094).

440 **References**

441 [1] J.R. Seymour, S.A. Amin, J.B. Raina, R. Stocker, Zooming in on the phycosphere:
442 the ecological interface for phytoplankton-bacteria relationships, Nat. Microbiol. 2
443 (2017). https://doi.org/10.1038/nmicrobiol.2017.65.

444 [2] L. Mekuto, A.V.A. Olowolafe, S. Pandit, N. Dyantyi, P. Nomngongo, R. Huberts,
445 Microalgae as a biocathode and feedstock in anode chamber for a self-sustainable
446 microbial fuel cell technology: a review, South African J. Chem. Eng. 31 (2020)
447 7–16. https://doi.org/10.1016/j.sajce.2019.10.002.

[3] Y. Cui, N. Rashid, N. Hu, M.S.U. Rehman, J.-I. Han, Electricity generation and microalgae cultivation in microbial fuel cell using microalgae-enriched anode and bio-cathode, Energy Convers. Manag. 79 (2014) 674–680. https://doi.org/10.1016/j.enconman.2013.12.032.

[4] C. Nagendranatha Reddy, H.T.H. Nguyen, M.T. Noori, B. Min, Potential applications of algae in the cathode of microbial fuel cells for enhanced electricity generation with simultaneous nutrient removal and algae biorefinery: current status and future perspectives, Bioresour. Technol. 292 (2019) 122010. https://doi.org/10.1016/j.biortech.2019.122010.

[5] B.E. Logan, K. Rabaey, Conversion of wastes into bioelectricity and chemicals by using microbial electrochemical technologies, Science (80-.). 337 (2012) 686–690. https://doi.org/10.1126/science.1217412.

[6] A. Elmekawy, H.M. Hegab, K. Vanbroekhoven, D. Pant, Techno-productive potential of photosynthetic microbial fuel cells through different configurations, Renew. Sustain. Energy Rev. 39 (2014) 617–627. https://doi.org/10.1016/j.rser.2014.07.116.

[7] F. Fischer, Photoelectrode, photovoltaic and photosynthetic microbial fuel cells, Renew. Sustain. Energy Rev. 90 (2018) 16–27. https://doi.org/10.1016/j.rser.2018.03.053.

[8] M. Rosenbaum, U. Schröder, Photomicrobial solar and fuel cells, Electroanalysis. 22 (2010) 844–855. https://doi.org/10.1002/elan.200800005.

469 [9] G. Yadav, I. Sharma, M. Ghangrekar, R. Sen, A live bio-cathode to enhance power
470 output steered by bacteria-microalgae synergistic metabolism in microbial fuel
471 cell, J. Power Sources. 449 (2020) 227560.
472 https://doi.org/10.1016/j.jpowsour.2019.227560.

473 [10] R. Kakarla, B. Min, Photoautotrophic microalgae *Scenedesmus obliquus* attached
474 on a cathode as oxygen producers for microbial fuel cell (MFC) operation, Int. J.
475 Hydrogen Energy. 39 (2014) 10275–10283.
476 https://doi.org/10.1016/j.ijhydene.2014.04.158.

477 [11] Z. Yang, H. Pei, Q. Hou, L. Jiang, L. Zhang, C. Nie, Algal biofilm-assisted
478 microbial fuel cell to enhance domestic wastewater treatment: nutrient, organics
479 removal and bioenergy production, Chem. Eng. J. 332 (2018) 277–285.
480 https://doi.org/10.1016/j.cej.2017.09.096.

481 [12] A. Commault, G. Lear, P. Novis, R. Weld, Photosynthetic biocathode enhances the
482 power output of a sediment-type microbial fuel cell, New Zeal. J. Bot. 52 (2014)
483 48–59. https://doi.org/10.1080/0028825X.2013.870217.

484 [13] X.W. Liu, X.F. Sun, Y.X. Huang, D.B. Li, R.J. Zeng, L. Xiong, G.P. Sheng, W.W.
485 Li, Y.Y. Cheng, S.G. Wang, H.Q. Yu, Photoautotrophic cathodic oxygen reduction
486 catalyzed by a green alga, *Chlamydomonas reinhardtii*, Biotechnol. Bioeng. 110
487 (2013) 173–179. https://doi.org/10.1002/bit.24628.

488 [14] B.E. Logan, R. Rossi, A. Ragab, P.E. Saikaly, Electroactivem microorganisms in
489 bioelectrochemical systems, Nat. Rev. Microbiol. 1 (2019).
490 https://doi.org/10.1038/s41579-019-0173-x.

[15] C. Li, S. Cheng, Functional group surface modifications for enhancing the formation and performance of exoelectrogenic biofilms on the anode of a bioelectrochemical system, Crit. Rev. Biotechnol. 39 (2019) 1015–1030. https://doi.org/10.1080/07388551.2019.1662367.

[16] S. Venkata Mohan, G. Velvizhi, P. Chiranjeevi, Microbial electrochemical platform: biofactory with diverse applications, in: Agarwal A, A. R., G. T., G. B. (Eds.), Green Energy Technol., Springer, Singapore, 2017: pp. 35–50. https://doi.org/10.1007/978-981-10-3791-7_3.

[17] L. Hall-Stoodley, J.W. Costerton, P. Stoodley, Bacterial biofilms: from the natural environment to infectious diseases, Nat. Rev. Microbiol. 2 (2004) 95–108. https://doi.org/10.1038/nrmicro821.

[18] G. Kumar, P. Bakonyi, G. Zhen, P. Sivagurunathan, L. Koók, S.H. Kim, G. Tóth, N. Nemestóthy, K. Bélafi-Bakó, Microbial electrochemical systems for sustainable biohydrogen production: surveying the experiences from a start-up viewpoint, Renew. Sustain. Energy Rev. 70 (2017) 589–597. https://doi.org/10.1016/j.rser.2016.11.107.

[19] L. Del Medico, D. Cerletti, P. Schächle, M. Christen, B. Christen, The type IV pilin PilA couples surface attachment and cell-cycle initiation in *Caulobacter crescentus*, Proc. Natl. Acad. Sci. 117 (2020) 9546–9553. https://doi.org/10.1073/pnas.1920143117.

511 [20] C.T. Kreis, M. Le Blay, C. Linne, M.M. Makowski, O. Bäumchen, Adhesion of
512 *Chlamydomonas* microalgae to surfaces is switchable by light, Nat. Phys. 14
513 (2018) 45–49. https://doi.org/10.1038/nphys4258.

514 [21] J.-H. Wang, L.-L. Zhuang, X.-Q. Xu, V.M. Deantes-Espinosa, X.-X. Wang, H.-Y.
515 Hu, Microalgal attachment and attached systems for biomass production and
516 wastewater treatment, Renew. Sustain. Energy Rev. 92 (2018) 331–342.
517 https://doi.org/10.1016/j.rser.2018.04.081.

518 [22] R. Jellali, J.C. Kromkamp, I. Campistron, A. Laguerre, S. Lefebvre, R.G. Perkins,
519 J.F. Pilard, J.L. Mouget, Antifouling action of polyisoprene-based coatings by
520 inhibition of photosynthesis in microalgae, Environ. Sci. Technol. 47 (2013) 6573–
521 6581. https://doi.org/10.1021/es400161t.

522 [23] H. Yuan, X. Zhang, Z. Jiang, X. Chen, X. Zhang, Quantitative criterion to predict
523 cell adhesion by identifying dominant interaction between microorganisms and
524 abiotic surfaces, Langmuir. 35 (2019) 3524–3533.
525 https://doi.org/10.1021/acs.langmuir.8b03465.

526 [24] C.T. Kreis, A. Grangier, O. Bäumchen, In vivo adhesion force measurements of
527 *Chlamydomonas* on model substrates, Soft Matter. 15 (2019) 3027–3035.
528 https://doi.org/10.1039/c8sm02236d.

529 [25] P. Geada, R. Rodrigues, L. Loureiro, R. Pereira, B. Fernandes, J.A. Teixeira, V.
530 Vasconcelos, A.A. Vicente, Electrotechnologies applied to microalgal
531 biotechnology – applications, techniques and future trends, Renew. Sustain.
532 Energy Rev. 94 (2018) 656–668. https://doi.org/10.1016/j.rser.2018.06.059.

[26] E. Marsili, J.B. Rollefson, D.B. Baron, R.M. Hozalski, D.R. Bond, Microbial biofilm voltammetry: direct electrochemical characterization of catalytic electrode-attached biofilms, Appl. Environ. Microbiol. 74 (2008) 7329–7337. https://doi.org/10.1128/AEM.00177-08.

[27] H.W. Harris, M.Y. El-Naggar, O. Bretschger, M.J. Ward, M.F. Romine, A.Y. Obraztsova, K.H. Nealson, Electrokinesis is a microbial behavior that requires extracellular electron transport, Proc. Natl. Acad. Sci. 107 (2010) 326–331. https://doi.org/10.1073/pnas.0907468107.

[28] M.-Y. Chen, D.-J. Lee, J.-H. Tay, K.-Y. Show, Staining of extracellular polymeric substances and cells in bioaggregates, Appl. Microbiol. Biotechnol. 75 (2007) 467–474. https://doi.org/10.1007/s00253-006-0816-5.

[29] R. Zhao, G. Chen, L. Liu, W. Zhang, Y. Sun, B. Li, G. Wang, Bacterial foraging facilitates aggregation of *Chlamydomonas microsphaera* in an organic carbon source-limited aquatic environment, Environ. Pollut. 259 (2020) 113924. https://doi.org/10.1016/j.envpol.2020.113924.

[30] B. Frølund, R. Palmgren, K. Keiding, P.H. Nielsen, Extraction of extracellular polymers from activated sludge using a cation exchange resin, Water Res. 30 (1996) 1749–1758. https://doi.org/10.1016/0043-1354(95)00323-1.

[31] B.-M. Wilén, B. Jin, P. Lant, The influence of key chemical constituents in activated sludge on surface and flocculating properties, Water Res. 37 (2003) 2127–2139. https://doi.org/10.1016/S0043-1354(02)00629-2.

554 [32] APHA, Standard methods for the examination of water and wastewater, 21st ed.,
555 American Publich Health Association, Washington, D.C., 2005.

556 [33] J. Gutman, S.L. Walker, V. Freger, M. Herzberg, Bacterial attachment and
557 viscoelasticity: physicochemical and motility effects analyzed using quartz crystal
558 microbalance with dissipation (QCM-D), Environ. Sci. Technol. 47 (2013) 398–
559 404. https://doi.org/10.1021/es303394w.

560 [34] T. Jafary, W.R.W. Daud, M. Ghasemi, B.H. Kim, J. Md Jahim, M. Ismail, S.S.
561 Lim, Biocathode in microbial electrolysis cell; present status and future prospects,
562 Renew. Sustain. Energy Rev. 47 (2015) 23–33.
563 https://doi.org/10.1016/j.rser.2015.03.003.

564 [35] D.F. Call, R.C. Wagner, B.E. Logan, Hydrogen production by *Geobacter* species
565 and a mixed consortium in a microbial electrolysis cell, Appl. Environ. Microbiol.
566 75 (2009) 7579–7587. https://doi.org/10.1128/AEM.01760-09.

567 [36] Y. Gu, H. Feng, X. Ying, K. Chen, J. Cheng, H. Huang, S. Zhen, D. Shen, Effects
568 of electrolyte conductivity on power generation in bio-electrochemical systems,
569 Ionics (Kiel). 23 (2017) 2069–2075. https://doi.org/10.1007/s11581-017-2047-4.

570 [37] S. Bajracharya, M. Sharma, G. Mohanakrishna, X. Dominguez Benneton,
571 D.P.B.T.B. Strik, P.M. Sarma, D. Pant, An overview on emerging
572 bioelectrochemical systems (BESs): Technology for sustainable electricity, waste
573 remediation, resource recovery, chemical production and beyond, Renew. Energy.
574 98 (2016) 153–170. https://doi.org/10.1016/j.renene.2016.03.002.

575 [38] H. Wang, Y. Shen, C. Hu, X. Xing, D. Zhao, Sulfadiazine/ciprofloxacin promote
576 opportunistic pathogens occurrence in bulk water of drinking water distribution
577 systems, Environ. Pollut. 234 (2018) 71–78.
578 https://doi.org/10.1016/j.envpol.2017.11.050.

579 [39] N. Zhu, L. Liu, Q. Xu, G. Chen, G. Wang, Resources availability mediated EPS
580 production regulate microbial cluster formation in activated sludge system, Chem.
581 Eng. J. 279 (2015) 129–135. https://doi.org/10.1016/j.cej.2015.05.017.

582 [40] G. Chen, N. Zhu, Z. Hu, L. Liu, G.-Q. Wang, G. Wang, Motility changes rather
583 than EPS production shape aggregation of *Chlamydomonas microsphaera* in
584 aquatic environment, Environ. Technol. 42 (2021) 2916–2924.
585 https://doi.org/10.1080/09593330.2020.1718216.

586 [41] A. Mishra, K. Kavita, B. Jha, Characterization of extracellular polymeric
587 substances produced by micro-algae *Dunaliella salina*, Carbohydr. Polym. 83
588 (2011) 852–857. https://doi.org/10.1016/j.carbpol.2010.08.067.

589 [42] L. Katarzyna, G. Sai, O.A. Singh, Non-enclosure methods for non-suspended
590 microalgae cultivation: literature review and research needs, Renew. Sustain.
591 Energy Rev. 42 (2015) 1418–1427. https://doi.org/10.1016/j.rser.2014.11.029.

592 [43] A. Ronen, W. Duan, I. Wheeldon, S. Walker, D. Jassby, Microbial attachment
593 inhibition through low-voltage electrochemical reactions on electrically
594 conducting membranes, Environ. Sci. Technol. 49 (2015) 12741–12750.
595 https://doi.org/10.1021/acs.est.5b01281.

596 [44] J. Allard, A. Mogilner, Traveling waves in actin dynamics and cell motility, Curr.
597 Opin. Cell Biol. 25 (2013) 107–115. https://doi.org/10.1016/j.ceb.2012.08.012.

598 [45] T.J. Jeon, R. Gao, H. Kim, A. Lee, P. Jeon, P.N. Devreotes, M. Zhao, Cell
599 migration directionality and speed are independently regulated by RasG and Gβ in
600 *Dictyostelium* cells in electrotaxis, Biol. Open. (2019) bio.042457.
601 https://doi.org/10.1242/bio.042457.

602 [46] G. Ramírez-García, L. Trapiella-Alfonso, F. D'Orlyé, A. D'Orlyé, Electrophoretic
603 methods for characterizing nanoparticles and evaluating their bio-interactions for
604 their further use as diagnostic, imaging, or therapeutic tools, in: Capill.
605 Electromigr. Sep. Methods, Elsevier, 2018: pp. 397–421.
606 https://doi.org/10.1016/B978-0-12-809375-7.00019-8.

607 [47] M. Hermansson, The DLVO theory in microbial adhesion, Colloids Surfaces B
608 Biointerfaces. 14 (1999) 105–119. https://doi.org/10.1016/S0927-7765(99)00029-
609 6.

610 [48] B.J. Kirby, E.F. Hasselbrink, Zeta potential of microfluidic substrates: 1. theory,
611 experimental techniques, and effects on separations, Electrophoresis. 25 (2004)
612 187–202. https://doi.org/10.1002/elps.200305754.

613 [49] A. Mantzorou, F. Ververidis, Microalgal biofilms: a further step over current
614 microalgal cultivation techniques, Sci. Total Environ. 651 (2019) 3187–3201.
615 https://doi.org/10.1016/j.scitotenv.2018.09.355.

616

Figure captions

Fig. 1 Schematic diagram of the laboratory-scale BES. Two 6 mm diameter plain graphite rods were connected to an electrochemical workstation by wires. A piece of carbon felt was attached onto the cathodic graphite rod to expand its working area.

Fig. 2 *C. microsphaera* cell attachment measurements (mean ± SD, n = 3) for various initial nitrate or phosphate concentrations and applied voltages in a microbial electrochemical system. ***, ** and * mark statistical significance of ANOVA test at $P<0.001$, $P<0.01$ and $P<0.05$, respectively.

Fig. 3 Nitrate and phosphate adsorptions (mean ± SD, n = 3) onto carbon felt electrodes for various initial nitrate or phosphate concentrations and applied voltages. Black dots represent experimental measurements, and curves and shaded areas with colors are linear fits and 95% confidence intervals for nitrate or phosphate concentration scenarios.

Fig. 4 Microalgal cell velocity measurements (mean ± SD, n >= 20) of *C. microsphaera* for various initial nitrate or phosphate concentrations and applied voltages at different times after inoculation, 20 min (red), 60 min (orange), 240 min (yellow), 480 min (green) and 720 min (royle blue). The crosspieces of the box plots (from right to left) are maximum, upper-quartile, median (black bar), lower-quartile, and minimum values, respectively. The individual points are outliers. ***, ** and * mark statistical significance of ANOVA test at $P<0.001$, $P<0.01$ and $P<0.05$, respectively.

638 **Fig. 5** Principal component analysis (PCA) of the multivariate variation among samples
639 at various applied voltages and different times after inoculation for (A) nutrient and
640 phosphate concentration of 250 mg/L; (B) nitrate concentration of 2.5 mg/L and (C)
641 phosphate concentration of 2.5 mg/L. Vectors indicate the direction and strength of
642 each variable to the overall distribution. PS, polysaccharide concentration; PN,
643 extracellular protein concentration; Adsorption, nitrate or phosphate adsorption onto
644 electrode; Zeta, zeta potential in the electrochemical system; Motility, cell velocity.

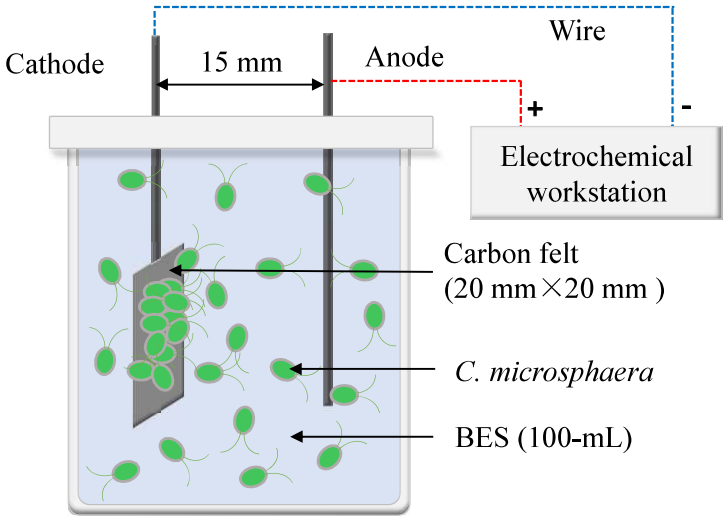
Wire
Cathode
15 mm
Anode
+
-
Electrochemical workstation
Carbon felt
(20 mm×20 mm)
C. microsphaera
BES (100-mL)

645

646 **Fig. 1**

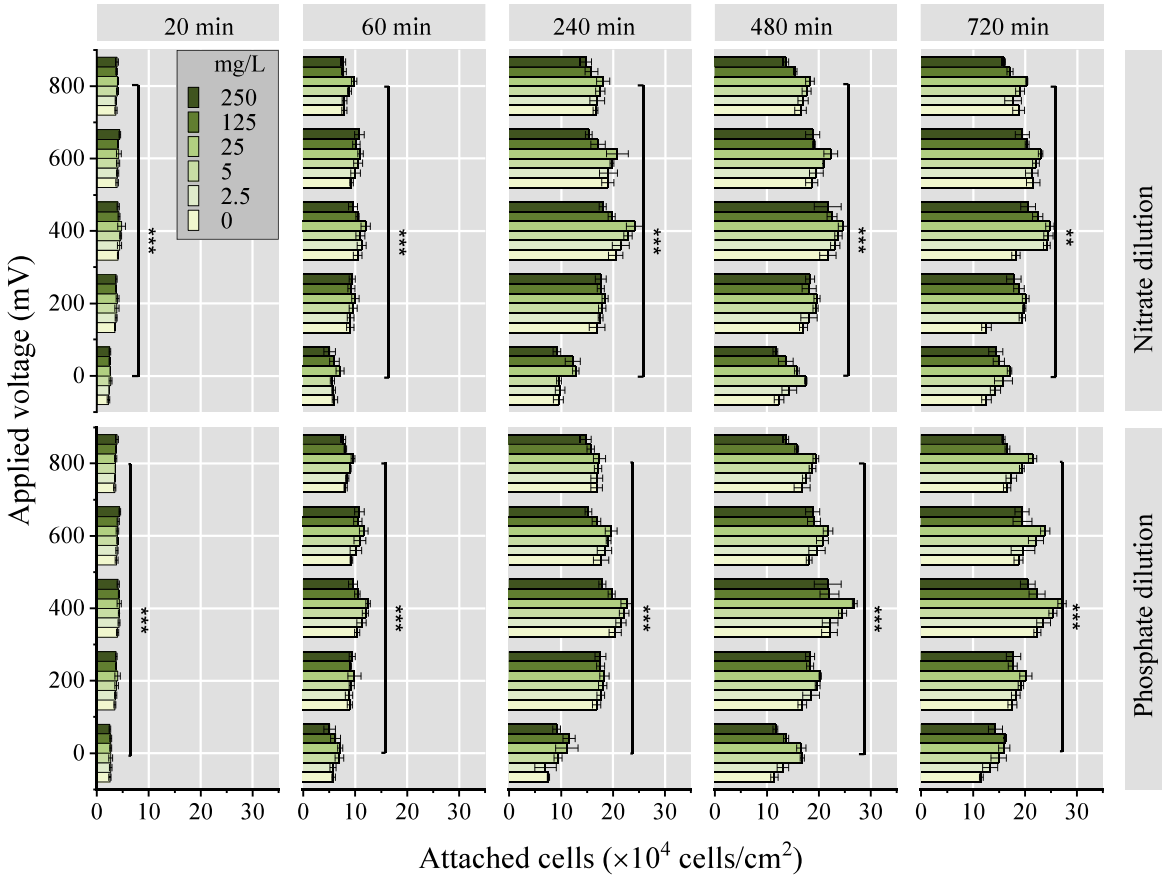
20 min
60 min
240 min
480 min
720 min
mg/L
250
125
25
5
2.5
0
Applied voltage (mV)
Attached cells (×10^4 cells/cm^2)
Nitrate dilution
Phosphate dilution
***
**

Fig. 2

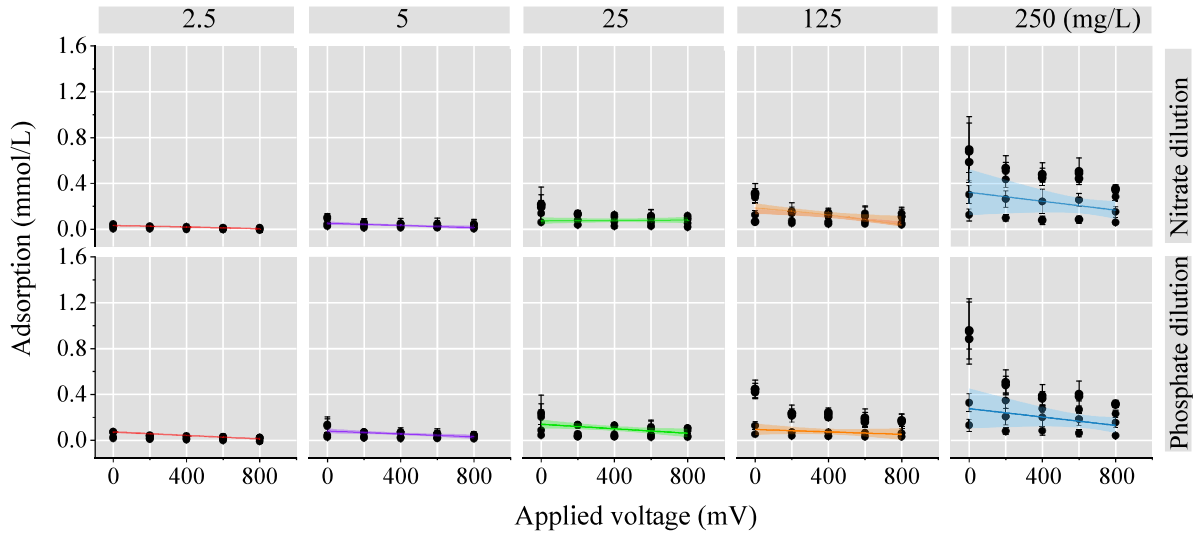
2.5
5
25
125
250 (mg/L)
Nitrate dilution
Phosphate dilution
Adsorption (mmol/L)
1.6
1.2
0.8
0.4
0.0
0
400
800
Applied voltage (mV)

649

650 **Fig. 3**

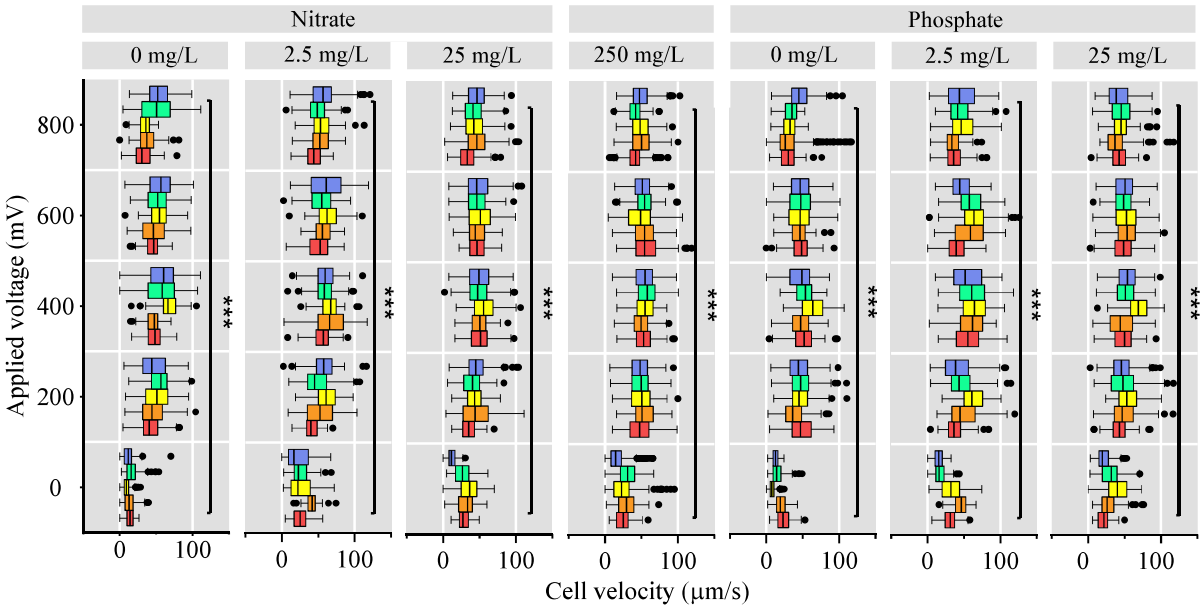
Nitrate
Phosphate
0 mg/L
2.5 mg/L
25 mg/L
250 mg/L
0 mg/L
2.5 mg/L
25 mg/L
Applied voltage (mV)
800
600
400
200
0
***
0
100
Cell velocity (μm/s)

651

652 **Fig. 4**

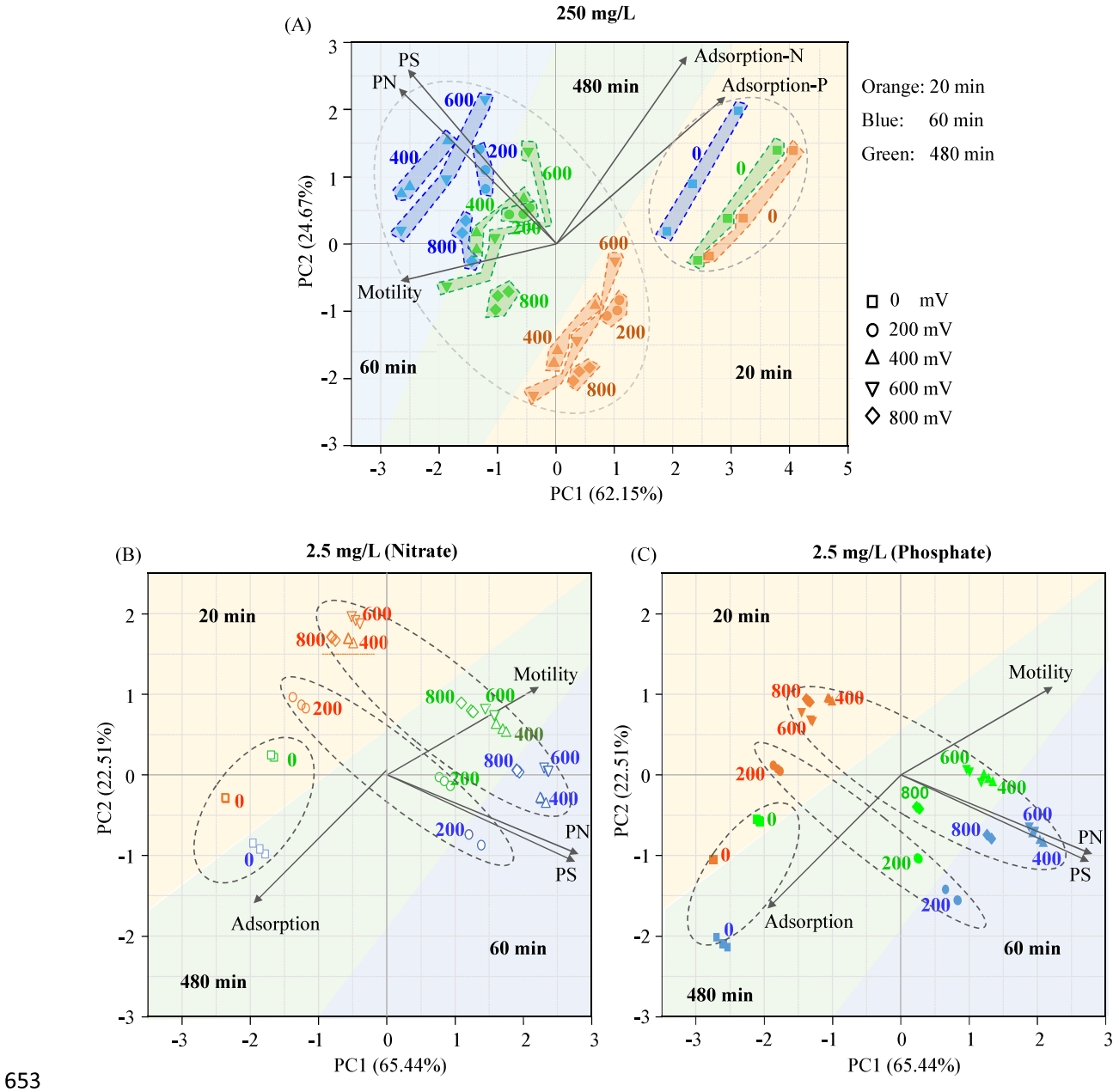
(A)
250 mg/L
PS
PN
480 min
Adsorption-N
Adsorption-P
Orange: 20 min
Blue: 60 min
Green: 480 min
Motility
60 min
20 min
0 mV
200 mV
400 mV
600 mV
800 mV
PC2 (24.67%)
PC1 (62.15%)
(B)
2.5 mg/L (Nitrate)
20 min
Motility
PN
PS
Adsorption
60 min
480 min
PC2 (22.51%)
PC1 (65.44%)
(C)
2.5 mg/L (Phosphate)
20 min
Motility
PN
PS
Adsorption
60 min
480 min
PC2 (22.51%)
PC1 (65.44%)

Fig. 5

Author Statement

Guowei Chen: Conceptualization, Investigation, Methodology, Reviewing and Editing. **Zhen Hu:** Investigation, Original draft preparation, Editing. **Ali Ebrahimi**: Reviewing and Editing. **David R. Johnson**: Reviewing and Editing. **Fazhu Wu:** Investigation, Original draft preparation. **Yifeng Sun:** Methodology, Editing. **Renhao Shen:** Investigation, Original draft preparation. **Li Liu:** Reviewing and Editing. **Gang Wang**: Conceptualization, Investigation, Methodology, Reviewing and Editing.